

# VISIBLE LIGHT PHOTOCATALYTIC DEGRADATION OF AQUEOUS METHYLENE BLUE BY Ni/Ti LAYERED DOUBLE HYDROXIDE

Priyadarshi Roy Chowdhury\* and Krishna G. Bhattacharyya  
*Department of Chemistry, Gauhati University, Guwahati-781014, Assam*  
\*For correspondence. (priyadarshiroychowdhury@yahoo.in)

**Abstract:** Visible light responsive Ni/Ti layered double hydroxide (LDH) was synthesized by a single step hydrothermal route using commercially available  $\text{Ni}(\text{NO}_3)_2 \cdot 6\text{H}_2\text{O}$ ,  $\text{TiCl}_4$  and urea which exhibited significant UV-visible absorption with a much narrower band gap (2.69 eV) that contributed significantly to the degradation of methylene blue under visible light. X-ray diffraction, Fourier transformed infrared spectroscopy (FT-IR) and  $\text{N}_2$  adsorption at 77 K were also carried out to investigate the structure and surface area of the sample. The photocatalytic degradation of aqueous methylene blue (MB) was observed due to the narrow band gap accompanied by comparatively high surface area. The photocatalytic activity improved in alkaline media particularly at pH 11 (catalyst dose  $0.075 \text{ gL}^{-1}$ ,  $1 \times 10^{-6} \text{ M MB}$ ). The catalytic activity was found to be higher than commercial catalysts like ZnO, ZnS,  $\text{TiO}_2$  and Degussa P25. Thus, this work demonstrated significantly photocatalytic properties of the Ni/Ti LDH in the field of environmental wastewater treatment.

**Keywords:** layered double hydroxide; band gap; photocatalysis; methylene blue; Degussa P25

## 1. Introduction:

Layered double hydroxides (LDHs), a class of anionic clays, have attracted considerable interest mainly because of their unique structure with variable metal cations in layer constituents as well as different exchangeable anions in galleries. They are widely used as polymer fillers and novel materials with magnetic, catalytic and photochemical functions. The variability of layered hydroxides arises from the combination of the inorganic hydroxide layers with the properties contributed by the host anions intercalated between these layers. Ultrathin nanosheets, prepared by delamination of layered hydroxides, have attracted attention due to the extremely small thickness of the order of 1 nm and large lateral size of the order of micrometers. Comparatively easy preparation, stability in air, interchangeable anions and incorporable host layers has made LDH an excellent precursor to develop novel photo functional materials. The general formula of these compounds is  $[\text{M}^{\text{II}}_{1-x}\text{M}^{\text{III}}_x(\text{OH})_2](\text{A}^{n-})_{x/n} \cdot y\text{H}_2\text{O}$ , where  $\text{M}^{\text{II}}$  and  $\text{M}^{\text{III}}$  represent divalent and trivalent cations, respectively and  $\text{A}^{n-}$  is the charge balancing anion. The surface charge can be tuned by varying the ratio of  $\text{M}^{\text{II}}/\text{M}^{\text{III}}$  and could be compensated by interlayer anions and water molecules [1-3]. The structural characteristics and compositional variability of the LDHs have potential applications in areas such as catalysts, catalyst supports and nanocomposites.

Ti containing LDHs have received much attention for their potential application in removal of toxic anionic substances from industrial wastewater. Methylene blue finds its uses in a range of different fields of chemistry such as printing, textile, and photographic industries. The dye is also known to cause irritation of the skin, eyes and the respiratory tract [3]. It is therefore important to eliminate these dyes from wastewater so that they do not foul natural water resources.

In the present work, the decolorization efficiency of the Ni/Ti LDH is evaluated by using methylene blue (MB), a model water-soluble dye which is widely used in chemical and textile industry. Thus, Ni/Ti LDH reported in the present work has proved itself to be an excellent candidate for removal of dye from water.

## 2. Experimental section:

### 2.1. Materials:

All the chemicals were of analytical grade and were used without further purification.  $\text{Ni}(\text{NO}_3)_2 \cdot 6\text{H}_2\text{O}$ ,  $\text{TiCl}_4$ ,

urea, ZnO, ZnS, Degussa P25 and methylene blue were purchased from Merck Chemicals Co. Ltd. USA. Deionized water (conductivity  $< 0.15 \text{ mS cm}^{-1}$ ) was used throughout the experiments.

## 2.2. Catalyst synthesis:

$\text{Ni}(\text{NO}_3)_2 \cdot 6\text{H}_2\text{O}$ ,  $\text{TiCl}_4$  as well as urea were used to prepare a hydrotalcite-like material by a co-precipitation method from homogenous solution. In a typical synthesis, 11.2 g of  $\text{Ni}(\text{NO}_3)_2 \cdot 6\text{H}_2\text{O}$ , 1.1 ml  $\text{TiCl}_4$  and 1.0 g urea were dissolved in 100 ml of deionised water at room temperature ( $\sim 30^\circ \text{C}$ ) and stirred vigorously for 2 h. The resulting mixture was aged in a Teflon lined autoclave at  $80^\circ \text{C}$  for 4 h. The green crystalline product so obtained was centrifuged, washed three times with water and dried.

## 2.3. Preparation of Methylene Blue solution:

Methylene blue (MB) dye (Figure 1) used in the photodegradation experiments was prepared by dissolving an accurately weighed amount in distilled water to a concentration of  $1 \times 10^{-4} \text{ M}$  (stock solution). The dye solutions of  $1 \times 10^{-5} \text{ M}$  and  $1 \times 10^{-6} \text{ M}$  were made by diluting the stock solution with appropriate amount of distilled water before the degradation experiments.



Figure 1: Structure of Methylene Blue.

## 2.4. Characterization techniques:

Powder X-ray diffraction (XRD) patterns were obtained with a PANalytical X'Pert PRO diffractometer that allowed both reflection and transmission experiments on the same sample. The XRD patterns were recorded between  $5$  and  $80^\circ$  ( $2\theta$ ) with a step size of  $0.013^\circ$  and an acquisition time of 30 s per step. Fourier Transform Infrared spectroscopy (FT-IR) measurements were recorded with a Shimadzu FT-IR 3000 spectrometer (resolution  $4 \text{ cm}^{-1}$ ), the sample was pressed into KBr disc with a weight ratio of sample to KBr of 1:100. The specific surface area, pore volume and pore size analyses were done with a Micromeritics TriStar 3000 V6.08 analyzer following Brunauer–Emmett–Teller (BET) and Barret–Joyner–Halender (BJH) methods. Prior to the measurements, the samples were degassed at  $120^\circ \text{C}$  for 3h. The solid UV–vis diffuse reflectance spectrum was recorded at room temperature with Hitachi U 4100 spectrometer using  $\text{BaSO}_4$  background. The absorption spectra in the photodegradation experiments were monitored by using a Shimadzu 1800 UV-Visible spectrometer.

## 2.5. Photocatalytic reactions:

The photocatalytic reactor consisted of a stainless steel chamber fitted with a 300 W tungsten lamp (Philips 38941-1; PS 25, Frost-6100) as the visible-light source, equipped with a wavelength pass filter ( $\lambda > 400 \text{ nm}$ ) at the bottom. The degradation experiments were performed with aqueous methylene blue (MB) at  $30^\circ \text{C}$  under vigorous stirring with a magnetic stirrer, taken in a double walled beaker with continuous circulation of running water separately through the outer jacket to ensure constant temperature of the reaction mixture. In all the degradation experiments, 150 ml of the reactants were vigorously stirred for 30 min in the dark to establish an adsorption/desorption equilibrium between the catalyst and the dye, followed by exposure to visible-light irradiation. 10 ml aliquots were sampled for analysis at 15 min intervals, centrifuged to remove solid catalyst particles and the centrifugate was analyzed for the unconverted dye using a Shimadzu UV-1800 spectrophotometer at  $\lambda_{\text{max}}$  of 664 nm. Reaction blank was carried out with the same procedure without adding catalyst. Moreover, the control reaction was also carried out in the dark with the catalyst for 75 min in order to evaluate its effect on the degradation process of MB. The effect of pH on the photocatalytic degradation was investigated by altering the pH value by 1 unit from pH 5 to 11. The pH values were adjusted by addition of hydrochloric acid or sodium hydroxide (0.1 M). The pH values were measured with a Systronics Digital pH meter (model 335, Systronics Analytical Instruments, India) and absorbances of the pH-adjusted solutions before and after the degradation process were measured in the manner described above. The effect of catalyst dose on degradation was investigated separately with 0.025, 0.05, 0.075, 0.1  $\text{g L}^{-1}$  of catalyst dose at pH 11 with

$1 \times 10^{-6}$  M MB solution. In order to evaluate the effect of dye concentration, the photocatalytic reactions were also performed with  $1 \times 10^{-4}$ ,  $1 \times 10^{-5}$  and  $1 \times 10^{-6}$  M MB solutions over  $0.075 \text{ gL}^{-1}$  of the catalyst at pH 11. A comparative photodegradation study was also performed using  $0.075 \text{ gL}^{-1}$  of commercially available pure ZnO, ZnS,  $\text{TiO}_2$  and Degussa P25 as reference samples with  $1 \times 10^{-6}$  M MB.

### 3. Results and discussion:

#### 3.1. X-ray diffraction analysis:

The LDH was characterized by powder X-ray diffraction (Figure 2) that revealed a typical layered structure similar to those previously reported in the literature for LDH-like materials [3-5]. In the present work, the diffraction peaks are in good agreement with the characteristic hexagonal phase of LDH. The (003), (006), (009) and (100) peaks appeared at  $13.32^\circ$ ,  $23.51^\circ$ ,  $38.34^\circ$  and  $31.62^\circ$  ( $2\theta$ ) respectively. The basal spacing corresponding to  $d_{(003)}$  was found to be  $0.763 \text{ nm}$  ( $2\theta \approx 13.32^\circ$ ) and that of  $d_{(110)}$  is  $0.153 \text{ nm}$  ( $2\theta \approx 27.12^\circ$ ). Since Ni/Ti LDH has been found to have the same basal spacing as in the normal LDHs, it is likely that the planar orientation of anions, mainly  $\text{CO}_3^{2-}$ , and  $\text{H}_2\text{O}$  molecules in the interlayer space has remained almost in a similar pattern in the LDH prepared in this work. The addition of  $\text{TiCl}_4$  in the aqueous media at room temperature during catalyst synthesis has generated  $\text{TiO}_2$  and is evident from the diffraction peaks in the XRD profile of the layered material. The diffraction peaks (110) and (101) at  $2\theta$  values of  $28.21^\circ$  and  $35.81^\circ$  in the LDH indicates the presence of  $\text{TiO}_2$  in the anatase phase as impurity, which is found to be in accordance with previous results. The XRD pattern also showed peaks at (0111), (018), (113) and (1013) which could be indexed to typical LDH materials. The narrow and sharp diffraction peaks indicate that the LDH material possesses good crystallinity. The contraction in the interlayer distance of Ni/Ti LDH is possibly related to strong electrostatic interactions between the host layer and the guest carbonate species in the presence of Ti.

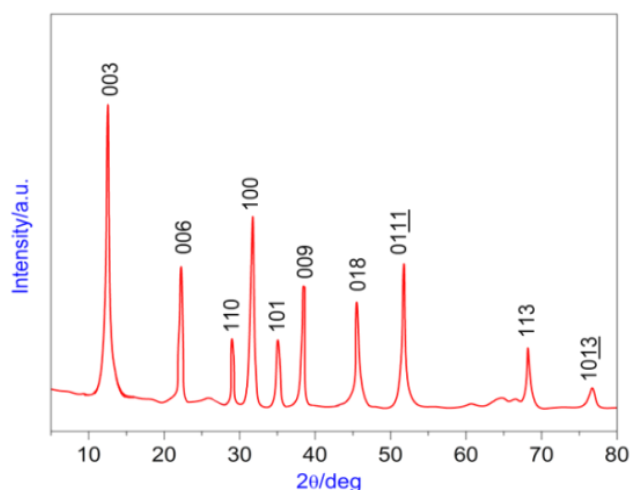


Figure 2: Powder X-ray diffraction of Ni/Ti LDH.

#### 3.2. FT-IR analysis:

The FT-IR spectrum recorded at room temperature showed the characteristic frequencies associated with the layered structure of the LDH materials (Figure 3). All the key bands resemble those exhibited by hydrotalcite-like phase with  $\text{CO}_3^{2-}$  as counter anion. An intense broad strong absorption band centered at  $3451 \text{ cm}^{-1}$  is attributed to the stretching vibrations of surface and interlayer water molecules and hydroxyl groups usually observed at lower frequency in the LDH rather than in the  $-\text{OH}$  stretching vibration in free water at  $3600 \text{ cm}^{-1}$ . This is related to the formation of hydrogen bonds of interlayer water with guest anions as well as with hydroxide groups of layers [4]. The broad band at  $3141 \text{ cm}^{-1}$  accompanied by a shoulder at near  $3023 \text{ cm}^{-1}$  can be assigned to the hydrogen bonding between water and carbonate in the interlayer. The band at  $1610 \text{ cm}^{-1}$  is assigned to the bending vibration of water molecules. In most of hydrotalcites, there are three IR active absorption bands arising from the carbonate anion observed at  $1385 \text{ cm}^{-1}$  ( $\nu_3$ ),  $1058 \text{ cm}^{-1}$  ( $\nu_1$ ) and  $745 \text{ cm}^{-1}$  ( $\nu_2$ ). The bands at approximately  $998$  and  $837 \text{ cm}^{-1}$  are attributed to stretching modes that confirm the presence of  $\text{NO}_3^-$  groups as impurity in the LDH interlayer with  $D_{3h}$  symmetry [5]. The sharp band at  $828 \text{ cm}^{-1}$  is associated with in-plane quadrant bending. Another peak at  $1110 \text{ cm}^{-1}$  is associated with C-O single bond stretching

vibrations. The band at approximately  $745\text{ cm}^{-1}$  is attributed  $\nu_2$  mode of the  $\text{CO}_3^{2-}$  species [3, 5]. The presence of all these bands, combined with XRD results, confirms that the materials have been successfully transformed into LDH via hydrothermal route.

### 3.3. $\text{N}_2$ sorption/desorption measurements:

In order to have an insight into the specific surface area and porosity of the LDH, low temperature  $\text{N}_2$ -sorption-desorption measurement was carried out (Figure 4). The BET isotherm belonged to Type IV with H3-type of hysteresis loop ( $p/p_0 > 0.4$  to  $\sim 0.8$ ). The considerably large hysteresis loop shows the condensation of  $\text{N}_2$  inside the pores and their release following reduction in pressure follow different paths, a characteristic of mesoporous structure of the material [4]. The Ni/Ti LDH thus consists of uniform mesopores formed through accumulation of particles. A broad pore size distribution is observed for the LDH sample with an average pore width of 5.13 nm [Figure 4 (inset plot)], which is likely to have been originated due to use of urea as template during the hydrothermal treatment. The BET specific surface area of  $232\text{ m}^2\text{g}^{-1}$  for the LDH could be considered as quite high due to which higher photocatalytic efficiency was observed. The BJH adsorption and desorption cumulative pore volume was 0.234 and  $0.218\text{ cm}^3\text{g}^{-1}$  respectively. The pore size distribution in the synthesized LDH is dominated by both micropores and mesopores in the diameter range of 0 – 10 nm. The mesoporous nature of the material with an appropriate spatial arrangement is likely to assist the electron/hole transfer within the framework and therefore, likely to be photo catalytically active.

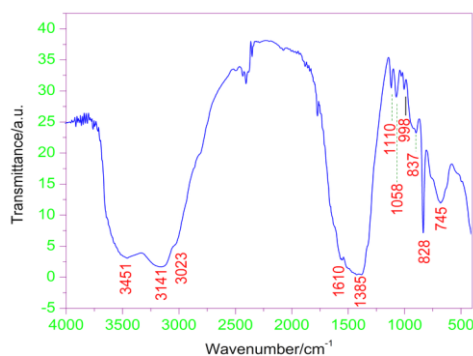


Figure 3: FT-IR spectrum of Ni/Ti LDH.

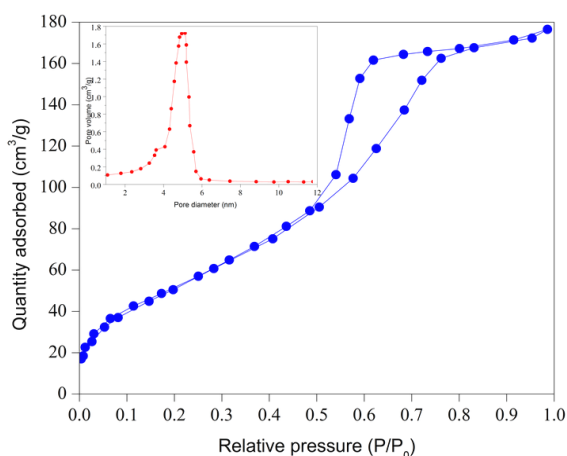


Figure 4:  $\text{N}_2$  sorption/desorption isotherm of Ni/Ti LDH.

### 3.4. Optical properties:

#### 3.4.1. Solid UV-vis DRS analysis:

The diffuse reflectance UV-vis analysis (Figure 5) was carried out to investigate the nature and coordination state of nickel and titanium incorporated in the layered framework. Two types of bands were identified:- ligand-to-metal charge-transfer (LMCT) band in the 200-350 nm range and d-d transition band from around 600-800 nm. Band assignments for the UV-vis spectra of Ni/Ti LDH reveals two bands in the 200-350 nm range, the

first centered at ~ 235 nm and the second centered at ~310 nm. The band at 235 nm could be assigned to an LMCT from O in OH<sup>-</sup> to an isolated Ni<sup>2+</sup> in octahedral coordination. This Ni<sup>2+</sup> is expected to be present in the brucite-like layers of LDH containing highly dispersed (isolated) Ni<sup>2+</sup> [2, 3]. The band at ~310 nm can be assigned to an LMCT from O in OH<sup>-</sup> to Ni<sup>2+</sup> in octahedral coordination corresponding to Ni–O(H)–Ni type of bonding. Besides this, a broad absorption band with maxima at ~550 nm that indicates the presence of Ti<sup>4+</sup> in the brucite like sheets [4]. The broad nature of absorption at ~550 nm could also be ascribed to supramolecular guest–guest (hydrogen bonding and van der Waals forces) or guest–host interactions (electrostatic attraction, hydrogen bonding and van der Waals forces). Meanwhile, a shoulder in the region 620-750 nm could be assigned to d–d transitions in Ni<sup>2+</sup> in a distorted (Jahn–Teller effect) octahedral structure. In case of the layered hybrid materials, the UV spectrum shows an overall broadening and a red shift is observed due to higher aggregate formation.

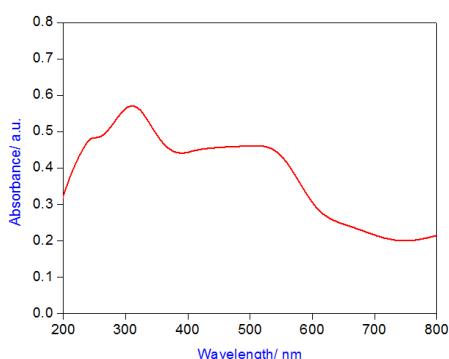


Figure 5: UV-Visible DRS of Ni/Ti LDH.

### 3.4.2. Comparative UV-VIS DRS analysis:

The solid UV-visible DRS spectra measured at room temperature for the synthesized Ni/Ti LDH and commercial catalysts like ZnO, ZnS, TiO<sub>2</sub> and Degussa P25 are shown in Figure 6. All of them showed strong absorbance ~270-460 nm. In addition to this, the synthesized LDH exhibits stronger absorption band from ~ 400-700 nm, which is not observed in any the commercial catalysts. The stronger absorbance in the visible region of the electromagnetic spectrum makes the Ni/Ti LDH, a potential candidate for degradation of dyestuffs under visible light than that of the commercial catalysts like ZnO, ZnS, TiO<sub>2</sub> and Degussa P25 [4, 5].

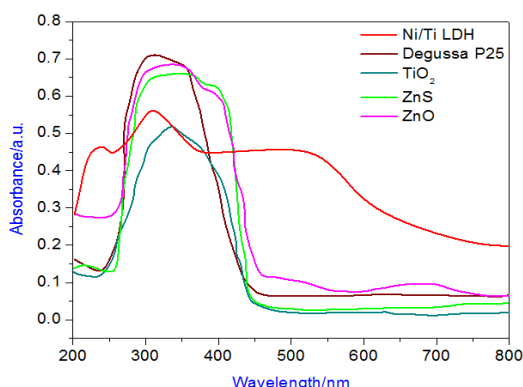


Figure 6. UV-Visible DRS spectra of Ni/Ti LDH with some important commercial catalysts.

### 3.4.3. Calculation of band gap:

UV–vis absorption measurement is a convenient and effective method for explaining the band structure of semiconductor materials. For a better understanding of the semiconducting properties of Ni/Ti LDH, the band gap of the Ni/Ti LDH and that of some commercial catalysts were measured from solid UV–Visible diffuse reflectance study (Figure 7) following the classical Tauc approach.

$$aE_p = K(E_p - E_g)^n \quad (1)$$

where,  $E_g$  represents the optical band gap,  $E_p$  is the photon energy,  $K$  is a constant and  $n$  depends on the nature of the transition. In fact,  $n$  assumes a value of 1/2, 3/2, 2, and 3 for direct allowed, direct forbidden, indirect allowed and indirect forbidden transitions respectively. In case of Ni/Ti LDH,  $E_p$  at  $a = 0$  gives absorption edge energies corresponding to  $E_g = 2.69$  eV which is much smaller than that of pure ZnO (~3.21 eV), ZnS (~3.54 eV),  $TiO_2$  (~3.22 eV) and Degussa P25 (~3.19 eV). The narrow band gap imparts better semiconducting properties to Ni/Ti LDH in comparison to photocatalysts like ZnO, ZnS,  $TiO_2$  and Degussa P25 [4, 5]. Moreover, the red shift in the UV-visible absorption spectrum of the Ni/Ti LDH is attributed to the narrow band gap. This suggests that pairs can be generated, even though the particle is irradiated with long wavelength-visible light. The decrease of band gap of the synthesized LDH can be attributed to the localized gap states induced by  $Ti^{3+}$  and oxygen vacancies that are responsible for its unique photocatalytic applications. Thus, Ni/Ti LDH material is expected to show more activity in the visible region of the electromagnetic spectrum and hence was used for dye degradation purpose under visible light.

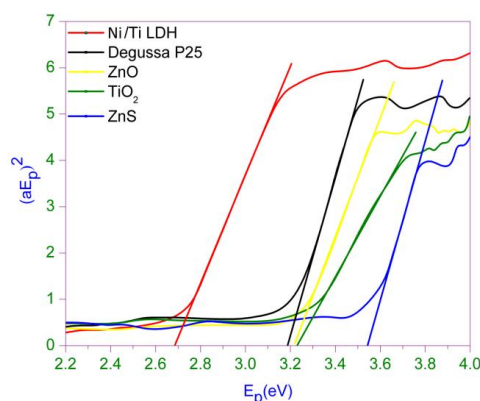


Figure 7. Tauc plot of Ni/Ti LDH with important commercial catalysts.

### 3.5. Photocatalytic reactions:

The photocatalytic activity of material is dependent on the surface area, narrow band gap, light harvesting ability by absorbing the incident photons with energies larger than its band gap energy ( $E_g$ ). The high specific surface area, narrow band gap as evident from BET and DRS analyses indicate that the synthesized LDH material could be induced easily with visible light, to produce more photo-induced carriers, resulting in high visible light photocatalytic activity. In the photocatalytic reactions, Ni/Ti LDH photocatalyst was dispersed in 200 ml aqueous solution of Methylene Blue (MB) and the mixture was stirred vigorously for 30 min in the dark for establishing adsorption equilibrium and then was exposed to irradiation under visible-light. The synthesized LDH exhibited better photocatalytic degradation of MB than commercial catalysts like ZnO, ZnS,  $TiO_2$  and Degussa P25. The degradation experiments were performed separately by varying the catalyst dose, dye concentration and pH. The photocatalytic degradation was estimated from the decrease in the absorption intensity of MB at  $\lambda_{max} = 664$  nm at 15 min intervals and the absorption spectra of the mixture were monitored as functions of irradiation time by using a UV-Vis spectrometer (Shimadzu 1800).

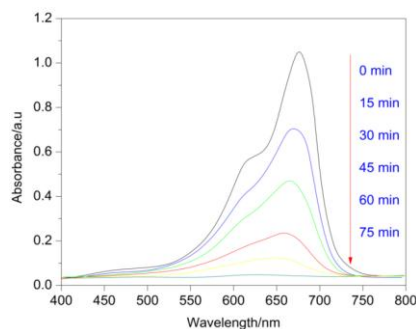


Figure 8. UV-visible absorption spectra involving the photo degradation of MB with Ni/Ti LDH (pH=11; 0.075 gL<sup>-1</sup> of catalyst; 1x10<sup>-6</sup> M MB solution).

The extent of the decomposition of the MB dye was obtained from the ratio,  $C/C_0$ , where  $C$  and  $C_0$  were the absorbances at a particular time interval and at  $t = 0$  respectively. It is seen that the strong absorption bands of MB decreased gradually upon increasing irradiation time and the absorbance of the dye solution was close to zero after 75 min of visible light irradiation for the synthesized LDH (Figure 8). In addition, the solution colour changed from an initial blue to nearly transparent at the end of the degradation. The enhanced photocatalytic activity of the synthesized Ni/Ti LDH, compared to ZnO, ZnS,  $TiO_2$  and Degussa P25 can be explained by the presence of high surface area, narrow band gap associated within the layered brucite like structure as supported respectively by BET, DRS and X-ray diffraction analyses. Blank (without catalyst) as well as dark reactions (in dark) were also performed under the same experimental conditions. Negligible degradation of MB was observed in the absence of the photocatalyst or visible light irradiation, which indicates that visible light plays a vital role in the degradation experiments.

### 3.5.1. Effect of photocatalyst dose:

The influence of catalyst dosage on decolorization of MB under visible light using Ni/Ti LDH catalyst was studied by varying the amount of catalyst between  $0.025$  to  $0.1 \text{ gL}^{-1}$  at  $1 \times 10^{-6} \text{ M}$  MB concentration (Figure 9). The results showed that on increasing the amount of catalyst from  $0.025$  to  $0.075 \text{ gL}^{-1}$ , an increase in decolorization efficiency was observed from 66% to 99.8% respectively. The increase in decolorization efficiency with increasing amount of catalyst dose in the reaction resulted from an increase in the available surface area or the active sites of the catalyst. However, the decrease in the degradation efficiency on increasing the catalyst load further to  $0.1 \text{ gL}^{-1}$  could be attributed to deactivation of activated molecules by collision with ground state molecules of the catalyst. Following this observation, the catalyst amount was kept to the value of  $0.075 \text{ gL}^{-1}$  in subsequent photocatalytic degradation experiments for obtaining maximum degradation efficiency.

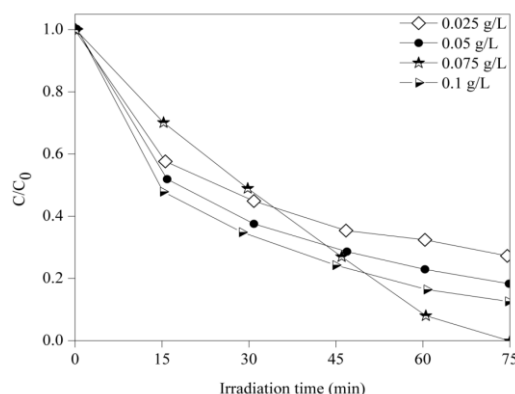


Figure 9. The effect of catalyst concentration on the photodegradation of MB (pH=11; MB concentration=  $1 \times 10^{-6} \text{ M}$ ).

### 3.5.2. Effect of pH:

The pH of the dye solution is an important parameter which controls the rate of degradation. In order to study the effect of pH, the degradation experiments were carried out using  $0.075 \text{ gL}^{-1}$  of catalyst;  $1 \times 10^{-6} \text{ M}$  MB solution (Figure 10) within the pH range of 5.0 to 11.0 by addition of either HCl or NaOH (0.1 M). The relationship  $C/C_0$  of aqueous MB was observed by varying pH and is presented in Figure 10. When the pH of the solution was increased from 5.0 to 6.0, the removal of MB increased from 36% to 41%. The maximum MB degradation of  $\sim 99.8\%$  was observed at pH 11.0, which is found to be in good agreement with the previous studies. The pH determines the surface charge on the catalyst surface. The degradation efficiency was found to be low in the acidic media. This is because at low pH, the  $H^+$  ion was considered to be a competitor to MB for adsorption sites on the surface of the catalyst. As a result, the degradation of MB could not be enhanced to a greater extent. However, in alkaline medium, at higher pH, the catalyst surface are likely to be electrostatically attracted to the MB molecules which has lead to the increase the degradation efficiency.

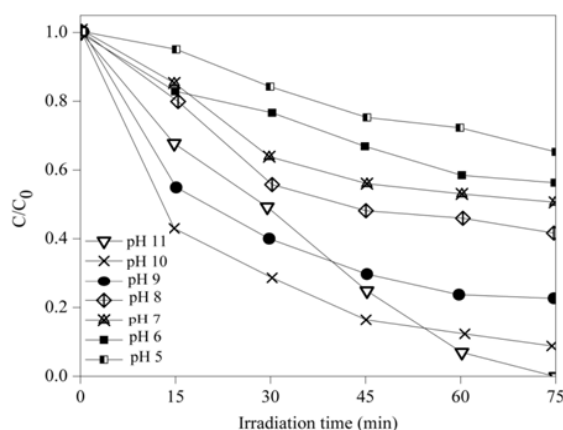


Figure 10. The effect of pH on photodegradation of MB (LDH dose= $0.075 \text{ gL}^{-1}$ ; MB concentration= $1 \times 10^{-6} \text{ M}$ ).

### 3.5.3. Effect of initial dye concentration:

It is important from mechanistic as well as application point of view to study the dependence of dye concentration on the photocatalytic degradation rate. The effect of initial MB dye concentration on the degradation rate was investigated in the concentration range of  $1 \times 10^{-4}$ ,  $1 \times 10^{-5}$  and  $1 \times 10^{-6} \text{ M}$ , maintaining the other reaction parameters constant (pH= 11; catalyst dose=  $0.075 \text{ gL}^{-1}$ ) (Figure 11). It is found that with  $1 \times 10^{-6} \text{ M}$  MB concentration  $\sim 99.8\%$  degradation was achieved. Beyond this concentration, the degradation rate decreased to 78% and 92% respectively for  $1 \times 10^{-4} \text{ M}$  and  $1 \times 10^{-5} \text{ M}$  MB. This may be due to the following factors: (i) higher dye concentration might serve as inner filter shunting the photons away from the catalyst surface (ii) non availability of oxidative free radicals (iii) more number of dye molecules get adsorbed on the catalyst surface thus blocking the surface active sites to participate in the degradation process. Thus, MB concentration was kept to  $1 \times 10^{-6} \text{ M}$  in photocatalytic degradation experiments for obtaining maximum efficiency.

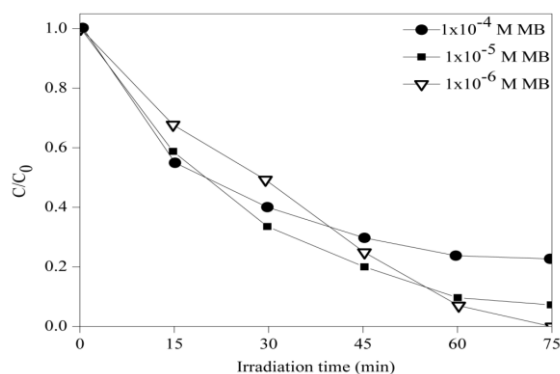


Figure 11. The effect of initial dye concentration on the photodegradation (pH= 11; catalyst dose=  $0.075 \text{ gL}^{-1}$ ).

### 3.5.4. Catalyst recyclability:

After each reaction run, the catalyst was separated from the reaction system and its reusability was also investigated carefully. The catalyst was washed three times with water, dried and reused. The degree of MB degradation for the first cycle was  $\sim 99.8\%$  (Figure 12). Although the degradation ability of the catalyst declined to  $\sim 97.5\%$ ,  $94.3\%$ ,  $91.2\%$  and  $88.1\%$  respectively for second, third, fourth and fifth cycles when they were reused again, the degradation rate still could amount to  $88.1\%$  after repeating fifth catalytic procedure, suggesting that the synthesized LDH is a potential recyclable candidate for dye degradation purposes.

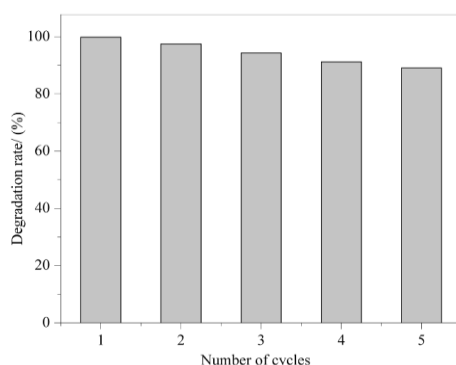


Figure 12. Number of cycles of aqueous MB photodegradation over Ni/Ti LDH.

### 3.5.5. Comparative study of the photocatalytic process:

A comparative study was undertaken to validate the influence of Ni/Ti LDH on photocatalytic activity of MB, (pH= 11; catalyst dose= 0.075 gL<sup>-1</sup>; MB concentration= 1x10<sup>-6</sup> M) which revealed an enhanced degradation of the aqueous MB over some important commercial catalysts like ZnO, TiO<sub>2</sub>, ZnS and Degussa P25 (Figure 13). The plot of C/C<sub>0</sub> versus irradiation time revealed that the Ni/Ti LDH displayed high photocatalytic activity under visible-light irradiation, reaches ~99.8 % in 75 min, in comparison to that of other commercial catalysts (ZnO ~59%, ZnS ~49%, TiO<sub>2</sub> ~43%, Degussa P25 ~71% degradation respectively). Thus, Ni/Ti LDH showed the highest photocatalytic activity in the visible light region than that of the commercial catalysts. Moreover, the blank reaction performed under the same set of experimental conditions without the catalyst showed ~15 % adsorption, as evident from the C/C<sub>0</sub> plot against time, is attributed to the effect of the visible light exposure on adsorption of the dye. However, the control experiments performed in the dark revealed ~23% adsorption as evident from the C/C<sub>0</sub> plot against time, indicating that visible light plays a major role in the degradation of aqueous methylene blue.

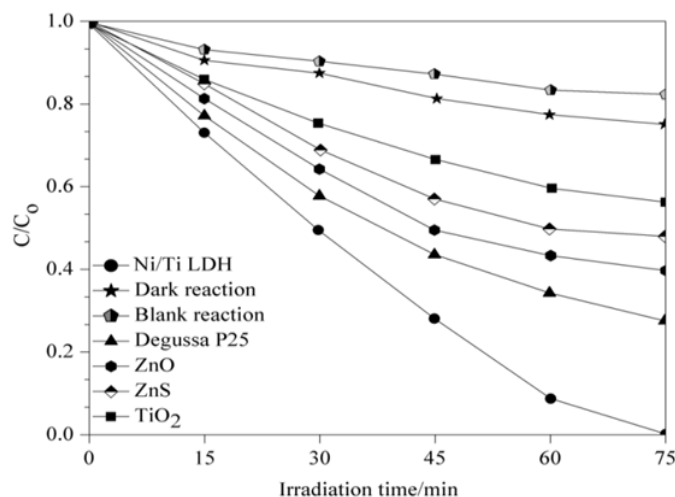
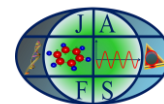


Figure 13. Plot of degradation of aqueous MB (C/C<sub>0</sub>) as a function of irradiation time for Ni/Ti LDH.

### 4. Conclusions:

In summary, Ni/Ti-LDH on urea substrate played a promising role as a semiconductor photocatalyst in which Ti atoms were dispersed homogeneously in the LDH lattice. The as-synthesized Ni/Ti-LDH has been found to exhibit remarkable photocatalytic activity for the degradation of aqueous methylene blue under visible light in comparison to that of some important commercial photocatalysts like ZnO, ZnS, TiO<sub>2</sub> and Degussa P25, due to its high specific surface area, porous structure and lower band gap as confirmed by BET/BJH, DRS, FT-IR and XRD observations. The photocatalytic activity improved in alkaline media particularly at pH 11, due to the electrostatic attractions between oppositely charged MB molecules and the Ni/Ti LDH. However, the catalyst retained its activity after five cycles of MB degradation and the FT-IR analysis of the catalyst before and at the



end of the fifth cycle showed excellent photostability. The strategy of applying urea solution as basic precipitant and adding homogeneously dispersed Ti atoms could be further extended to other transition metal-based oxide/hydroxide thin films to enhance their photocatalytic properties. Therefore, it is expected that the Ni/Ti LDH in this work could be potentially used as an effective and recyclable photocatalyst for large scale environmental wastewater treatment.

References:

- [1] Z.P. Xu, J. Zhang, M.O. Adebajo, H. Zhang and C. Zhou, *Applied Clay Science*, 53, 139, 2011.
- [2] X. Xiang, L. Zhang, H. I. Hima, F. Li and D.G. Evans, *Applied Clay Science*, 42, 405, 2009.
- [3] P. R. Chowdhury and K.G. Bhattacharyya, *Dalton Transactions*, 44, 6809, 2015.
- [4] J. Zhang, D. Fu, H. Gao and L. Deng, *Applied Surface Science*, 258, 1294, 2011.
- [5] Y.F. Zhao, M. Wei, J. Lu, Z.L. Wang and X. Duan, *ACS Nano*, 3, 4009, 2009.